RSC Advances

ROYAL SOCIETY OF CHEMISTRY

www.rsc.org/advances

ARTICLE TYPE www. rsc.org/xxxxxx | XXXXXXXX

Effects of strain on band gap and effective mass in two-dimensional monolayer GaX (X=S, Se, Te)†

Le Huang,[a] Zhanghui Chen,[a] and Jingbo Li,*[a]

Received Xth XXXXXXXXXX 20XX, Accepted Xth XXXXXXXXX 20XX
First published on the web Xth XXXXXXXXXX 200X
DOI: 10.1039/b000000x

First-principles calculations are performed to study the mechanical and electronic properties of two-dimensional monolayer GaX (X = S, Se, Te) under strain. It is found that the in-plane stiffness decreases from 86 N/m for GaS, 68 N/m for GaSe to 57 N/m for GaTe, agreeing well with experimental results and it is attributed to the weakening interaction between Ga and X atoms with the increasing atomic number of X atoms. The band gaps of GaX monolayers decrease approximately linearly with increasing tensile strain, while the variation of band gaps with compressive strain does not show a linear feature because the conduction band maximum transfers among several high symmetry k-points. The effective masses of electrons and holes also exhibit strong anisotropy and can be modulated by applying both compressive and tensile strains, indicative of monolayer GaX very useful for device modeling.

1 Introduction

Two-dimensional nanomaterials such as graphene, transition metal dichalcogenide(TMD) and boron nitride have been widely studied due to their remarkable physical properties and numerous promising applications [1–5]. Among these, graphene has been the most extensively studied because of its high mobility and rich physics and its electronic properties can be controlled by a gate electrode [2,6,7]. Its applications, however, are hindered by the absence of band gap in pristine graphene. In order to achieve different applications, modifications of their intrinsic properties are often required. For example, a broad range of chemical decoration [8,9] and substitutional doping [10,11] have been investigated to open and tune the band gap of graphene. It has been demonstrated both experimentally and theoretically that the band gap and optical properties of graphene can be controlled and tuned by applying strain [12,13]. Monolayer TMDs such as molybdenum disulfide(MoS_2) are ideal candidates for using strain engineering as an effective tool to modify their electronic and magnetic properties [14–17]. Besides, lattice point defects can act as very efficient traps for electrons, holes and excitons, and strongly influence transport and optical properties of the host materials [18].

Very recently, a stable class of two-dimensional metal dichalcogenide materials, GaX(X = S, Se, Te) monolayers, has been extensively studied due to their potential applications as photodetectors, gas sensors and optoelectronic devices. Monolayer GaS and GaSe sheets have already successfully been synthesized [19–22]. Compared to graphene, monolayer GaX are intrinsically semiconducting materials with wide band gaps. Each layer of GaX consists of four covalently bonded X-Ga-Ga-X atoms, as illustrated in Fig.1. Experiments show evidence that monolayer GaS and GaSe are perfect candidates for using in field-effect transistors [21]. Aside from these intriguing features, GaX monolayer show promising applications for nanophotonic devices [19]. Much effort has been made to study the structural, elastic and electronic properties of GaX. Also, the band gap of GaX monolayer can be widely tuned by applying mechanical deformation [23]. Accurate hybrid functional and quasiparticle methods predict that the GaX are suitable photocatalysts for water splitting [24]. Although the response of band gap of GaS and GaSe to uniaxial and biaxial strain has been recently calculated, other properties such as effective masses have not been considered yet. Besides, how the band gaps of GaX would behave under compressive strains has not been examined. What is more, the compressive strain can be easily realized in the experiments. These issues, actually, play important role in interpretation of experiments and device modeling. In order to address these issues, a systematic investigation of strain effects on the electronic properties and effective masses of GaX would be highly desirable.

In this work, we study the electronic the mechanical and electronic properties of GaX monolayers, but focus on their carrier effective mass and possible implications enabled by the carrier effective mass. We calculate the elastic parameters of GaX including in-plane stiffness and Poisson's ratio. Band gaps of GaX are discussed by both GGA and hybrid functional calculations. The band gaps of GaX can be reduced

[a] *State Key Laboratory for Superlattice and Microstructures, Institute of Semiconductors, Chinese Academy of Sciences, Beijing 100083, China. E-mail: jbli@semi.ac.cn*

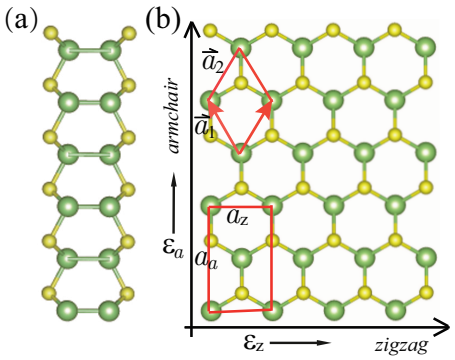

Fig. 1 (color online) (a) Side view and (b) Top view of monolayer GaX. The green and yellow balls denote Ga and chalcogenide atoms, respectively. The rectangular and rhombic regions present the unit cells used to calculate the elastic and electronic properties, respectively. ε_a and ε_z are the strain along the armchair and zigzag directions with respect to the lattice constant, respectively.

by both homogeneous tensile (H-strain) and uniaxial tensile strains along zigzag (Z-strain) either armchair direction (A-strain), compressive strains tend to show much less influence on the band gap than tensile strains. We also calculate the variation of effective masses of carriers in GaX with H-strain.

2 Methods

The calculations are performed using the projector augmented wave (PAW) method[25] with the generalized gradient approximation of Perdew-Burke-Ernzerhof (GGA-PBE)[26] exchange-correlation functional and the Heyd-Scuseria-Ernzerhof (HSE06) hybrid functional[27]. A $(9 \times 9 \times 1)$ Monkhorst-Pack[28] k-point grid and a plane-wave basis set with an energy cutoff of 500 eV are used for all calculations. A large vacuum layer of more than 12 Å is adopted to prevent the interaction between adjacent images. All the structures are fully relaxed with a force tolerance of 0.02 eV/Å. Numerical calculations are implemented by the Vienna ab initio simulation package (VASP)[29].

3 Results and Discussion

3.1 Mechanical Properties

We first present the structural parameters of the single-layer GaX (Fig.1) with PBE functionals, as shown in Table 1. The optimized lattice constants of 3.63 Å for GaS, 3.82 Å for GaSe and 4.13 Å for GaTe by GGA-PBE functional are consistent with previous studies[24]. These values are a little larger than the ones (3.59 Å for GaS, 3.75 Å for GaSe) in bulk[30,31]. For the X and Ga bonds are strong ionic, the transfer charge from

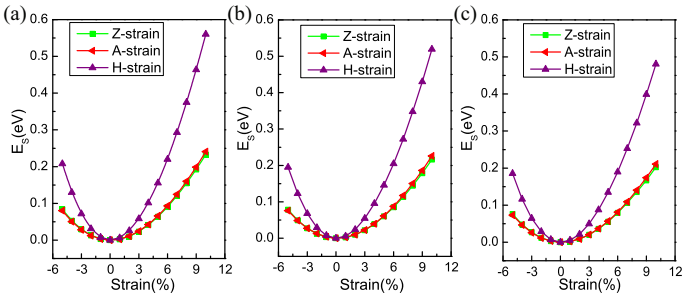

Fig. 2 (color online) The evolution of strain energy E_s of (a) GaS, (b) GaSe and (c) GaTe with strains.

the Ga to the X atom can reflect the strength of the X and Ga bonding. Bader charge analysis shows that there are a little more charge transferred from Ga to X atoms in the 3D GaX semiconductors (0.8150 e transferred to each S atom in GaS monolayer) than that in the 2D counterparts (0.8104 e transferred to each S atom in GaS bulk). Stronger bonding between Ga and X atoms in bulk GaX leads to a shorter Ga-X bonds and smaller lattice constants.

Next, we discuss the strain energy before analyzing elastic properties of GaX. Strain energy gives an insight into the influence of strain on the structural and elastic properties and it can be illustrated as $E_S = E_T(\varepsilon) - E_T(\varepsilon = 0)$, where $E_T(\varepsilon)$ is the total energy at a given axial strain ε and $E_T(\varepsilon = 0)$ is the total energy at equilibrium state. The evolution curves of strain energy of GaS, GaSe and GaTe with three types of strains illustrated above are shown in Fig.2. For both tensile and compressive strains within the loaded range, the strain energy increases monotonously with the corresponding increasing strain. The harmonic approximation is well applied with $-0.02 < \varepsilon < 0.02$, beyond which the $E_s - \varepsilon$ curve becomes inharmonic because the contributions of higher order terms are larger than 10% and noticeable.

All the curves show their minima at zero strain. It is clear that the A-strain and Z-strain exert almost the same influence on the strain energy of GaX. This can be attributed to the hexagonal lattices with honeycomb structures of GaX monolayer. Their mechanical properties including in-plane stiffness are isotropic even under small strains, which results in the equal contribution of intralayer interaction between Ga and X atoms along both A-direction and Z-direction. From the atomic configuration of GaX in Fig.1, we can see that the intralayer interaction mainly comes from the Ga-X bonding. The three Ga-X bonds for each X atom make the equal contribution along A-direction and Z-direction.

We now study the elastic properties of GaX, which are usually characterized by two independent constants: Young's modulus Y and Poisson's ratio ν. However, it is difficult to calculate the thickness of the sheet system which is re-

Table 1 The structural parameters and elastic parameters of single-layer GaX on GGA-PBE level. d_1 and d_2 are the distance between two Ga atoms and two X (X = S, Se, Te) atoms, respectively. t_1, t_2 are the fitting parameters. ν and C are the Poisson' Tatio and in-plane stiffness, respectively.

	d_1 (Å)	d_2 (Å)	a_0 (Å)	t_1	t_2	ν	C (N/m)
GaS	4.63	2.47	3.63	32.75	12.67	0.244	85.87
GaSe	4.82	2.47	3.82	28.15	12.53	0.248	67.14
GaTe	5.02	2.47	4.13	26.16	12.9	0.246	56.46

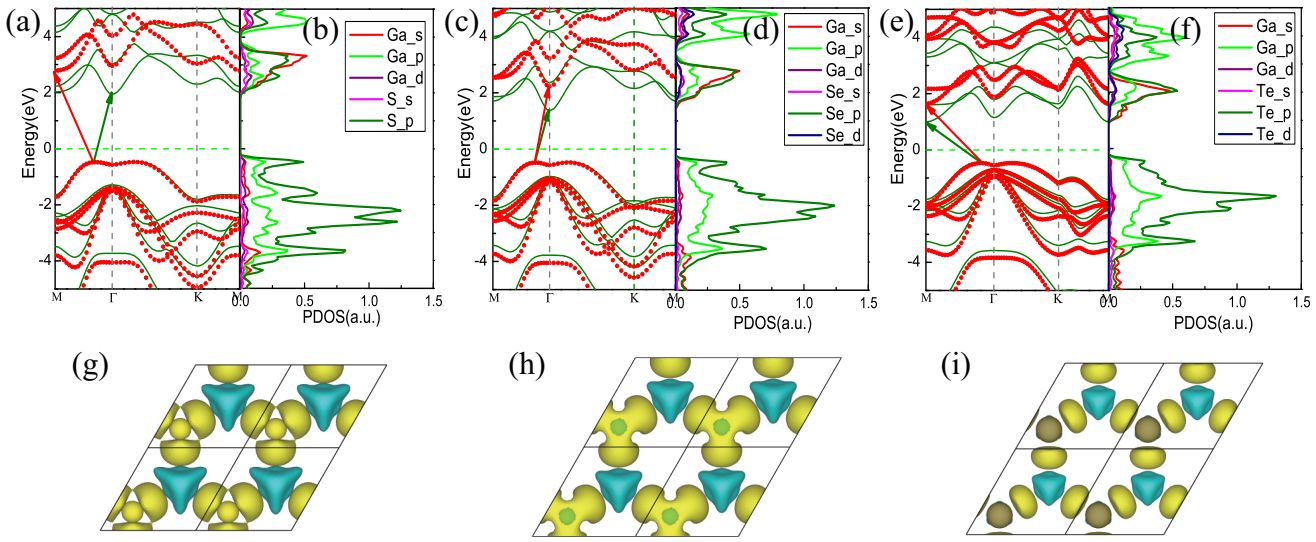

Fig. 3 (color online) Band structures and the projected density of states of monolayer GaX without strain are shown in (a)-(e). Solid line and filled circle in band structures represent the GGA-PBE and HSE06 calculated results. The solid arrows indicate the lowest energy transition. (g)-(i) show the charge redistribution of GaS, GaSe and GaTe, respectively.

quired in calculating the Young's modulus. Calculating the in-plane stiffness is an alternative way with respect to Young's modulus. The in-plane stiffness C can be defined as $C = (1/S_0)(\partial^2 E/\partial\varepsilon^2)$, where S_0 is the equilibrium area, E is the total energy, and ε is uniaxial strain ($\varepsilon = \Delta a/a$). The other parameter, Poisson's ratio ν, is the ratio of transverse strain and axial strain, namely, $\nu = -\varepsilon_{strans}/\varepsilon_{axial}$. To calculate the elastic properties of GaX, we construct a rectangular unit cell of GaX, which contains two GaX molecules, as seen in Fig.1[32–34]. In our calculations, the two lattice constants, a_z and a_a, are changed by -2% to 2% in an increment of 1%. The system is fully re-optimized and the corresponding total energy is obtained at each (ε_a, ε_z) point. Afterwards, the total energy can be written as $E = t_1{\varepsilon_z}^2 + t_1{\varepsilon_a}^2 + t_2\varepsilon_z\varepsilon_a + E_0$, in which E_0 is the total energy at equilibrium state; ε_z and ε_a are the strains along zigzag and armchair directions, respectively; t_1 and t_2 are related coefficients. The in-plane stiffness and Poisson's ratio finally can be calculated by $C = (1/S_0)(2t_1 - {t_2}^2/2t_1)$ and $\nu = t_2/t_1$.

Table 1 gives the fitting parameters t_1 and t_2 as well as elastic constants C and ν. These elastic parameters are determined by using the method based on strain energy calculation in the harmonic elastic deformation range. The in-plane stiffness C of GaS, GaSe and GaTe are 86, 68 and 57 N/m, respectively. Also, their Poisson's ratios are 0.244, 0.248 and 0.246. The calculated results of in-plane stiffness C agree well with the reported results of 98 N/m for GaS, 79 N/m for GaSe and 66 N/m for GaTe[24]. It is clear that the in-plane stiffness degrades with increasing atomic number of chalcogenide atoms, whereas the Poisson's ratio varies by a small amount among them. From the formula of in-plane C, we can see that the C is dominated by t_1 when t_1 is larger than t_2. t_1, to some extent, reflects the strength of intralayer interaction of GaX monolayer. With the increasing atomic number of chalcogenide atoms, the bonding between Ga atoms and chalcogenide atoms becomes weaker, leading to a smaller t_1 and relatively smaller in-plane stiffness.

In order to gain further insight, the binding energy of a chalcogenide atom in GaX monolayer is calculated and presented in Table 2. We construct a supercell containing $4\times4\times1$ unit cells in binding energy calculations. The binding energy is defined as the difference between the total energy of a GaX supercell and the sum of total energy of a GaX supercell with a vacancy at chalcogenide atom site and that of an isolated chalcogenide atom:

$$E_b = E_{supercell} - E_{withvacancy} - E_{chalcogenide}.$$

where $E_{supercell}$ and $E_{withvacancy}$ are the total energies per unit cell of the supercell without and with a vacancy at chalcogenide atom site, respectively; $E_{chalcogenide}$ is the energy of an isolated chalcogenide atom. Consistent with the above analysis, with the increasing atomic number of chalcogenide, its binding energy in the corresponding GaX monolayer numerically decreases, which implies the weakening bonding between X atoms and Ga atoms with X changing from S to Te. Furthermore, as the Ga-Ga bonds are perpendicular to the plane of GaX monolayers, the bonds between Ga atoms and X atoms make the main contribution to the in-plane stiffness. It can be concluded that the stronger binding between Ga atoms and chalcogenide atoms results in the larger in-plane stiffness.

3.2 Electronic properties

We next study the band structures of the unstrained GaX monolayers by both PBE and HSE06 calculations. As shown in Fig.3(a), (c) and (e), all the three monolayers are indirect-band-gap semiconductors. Their band gaps calculated on PBE and HSE06 level are listed in Table.2. The general feature of the band structures calculated by PBE and HSE06 is similar, except that the band gap calculated by HSE06 is much larger than the other because PBE usually underestimate band gaps. Our results are in great agreement with previous results[23,24].

In order to determine the constituents of the electronic bands, the projected density of states (PDOSs) are also calculated by PBE functional and shown in Fig.3(b), (d), and (f). Each of them shows a gap near the Fermi level, which is smaller than the corresponding value of band structure calculation due to the shift of the conduction band minimum (CBM) and the valence band maximum (VBM) towards the Fermi level. For the unstrained GaS, the CBM and the VBM are mainly constituted by $S-p$ states and $Ga-p$ states.

From Fig.3 and Table.2, it is found that the band gap of unstrained GaX monolayer decreases as we go down the column of X atoms in the periodic table. This is possibly caused by the increasing delocalization of the atomic orbitals, which leads to reduced interaction between Ga and X atoms and elongated lattice constant. These conclusions are further supported by the redistribution of charges, which is calculated by taking the difference of the total charge of the GaX and the sum charge of isolated chalcogenide and Ga atoms, as shown in Figs.3(g)-(i). In the GaX monolayers, the Ga-X bond is strongly ionized, the delocalization could reflect the strength of the atomic interaction, similar to the TMDs[35–37]. In this work, the GaS monolayer shows the maximum redistribution of the charge of the three GaX monolayers. More transferred charge from Ga atom to chalcogenide atom and shorter lattice constant of GaS lead to stronger interaction between Ga and S atoms.

We now study the behavior of band gap of GaX under strain by using GGA-PBE. We consider three types of strain: uniform biaxial strain (H-strain), uniaxial strain along armchair direction (A-strain) or zigzag direction (Z-strain). Fig.4 presents the Brillouin zone (BZ) of GaX monolayers under strain. The irreducible BZ of GaX under H-strain remains un-

Table 2 The binding energy (E_b) of chalcogenide atoms in GaX monolayers on GGA-PBE level and the band gaps of these monolayers on both GGA-PBE and HSE06 level are listed here. The average charge of every atom of GaX at equilibrium state is given too.

	E_b (eV)	Charge of X	Charge of Ga	Band gap (PBE, eV)	Band gap (HSE06, eV)
GaS	-6.963	6.8104	12.1896	2.48	3.19
GaSe	-6.354	6.6615	12.3385	1.83	2.71
GaTe	-5.709	6.4438	12.5562	1.44	2.02

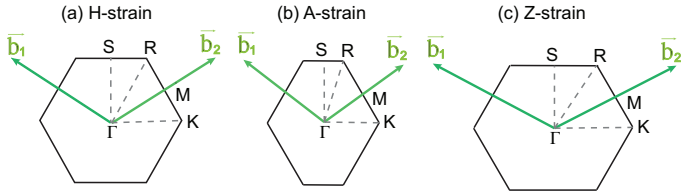

Fig. 4 (color online) Brillouin zone with high-symmetry points of monolayer GaX under (a) H-strain, (b) A-strain and (c) Z-strain.

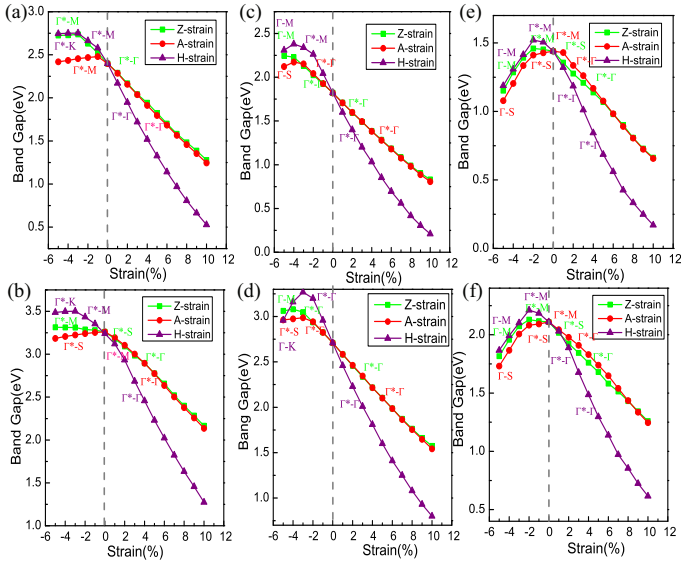

Fig. 5 (color online) (a), (c) and (e) show the GGA-PBE results of variation of band gaps of GaS, GaSe and GaTe versus strains, respectively. The below panels correspond to HSE06 results. Γ^* denotes the maximum points of valence band which locate at the side of Γ point and the label of $k-k^*$ along each curve denotes that the VBM and CBM locate at k point and k^* point, respectively under corresponding strain.

changed, as the hexagonal symmetry is saved. In Fig.4 (a), the R point and S point are equivalent to K point and M point, respectively. In the case of A-strain and Z-strain, the structure of the BZ is deformed as the hexagonal symmetry is degenerated to rhombic symmetry, and the irreducible BZ becomes a right trapezoid from the original triangular shape. Moreover, the high-symmetry k-point increase from three (Γ, K, M) to five (Γ, K, M, R, S).

We constrain the tensile strain within the range from 0 to 10% in our calculations and a small compressive strain ranging from -5% to 0 is imposed. The variation of the band gaps of GaX calculated by GGA-PBE as a function of strain is summarized in Fig.5. Γ^* denotes the maximum points of valence band which locate at the side of Γ point and the label of $k-k^*$ along each curve denotes that the VBM and CBM locate at k point and k^* point, respectively under corresponding strain. In the case of tensile strain, the band gaps of GaX decrease approximately linearly. While the variation of band gaps with compressive strain does not show linear feature because the conduction band maximum transfers among several high symmetry k-points. Take GaS under H-strain as an example, its variation of the band gap calculated by PBE is plotted by violet line in panel (a) of Fig.5. The CBM and VBM is marked along the curve. Under tensile strain, the curve is marked by Γ^*-Γ, which means the VBM locates at Γ^* point and CBM locates at Γ point. When under compressive strain, the VBM remains at Γ^* point. The CBM, however, transfers from Γ point to M point, then to K point. On the other hand, A-strain and Z-strain exert similar influence on the band gap of GaX. All the results show that the band gaps of GaX can be modified over a wide range by applying tensile strain.

We check the variation of the band gaps of GaX with applied strains by calculating the band structures using the HSE06 functional method, which also is shown in Fig.5. Although the calculated HSE06 band gaps of GaX are larger than the PBE ones, the nature of the band structure remained unchanged.

A decreasing band gap of GaX with increasing tensile strain implies reduced interaction between Ga and X atoms, which should be caused by increasing distance between them. Due to the increase of the chalcogen atomic radius, the bond length of Ga and X atom also increase in the sequence of GaS $<$ GaSe $<$ GaTe, which results in weakening bonding between

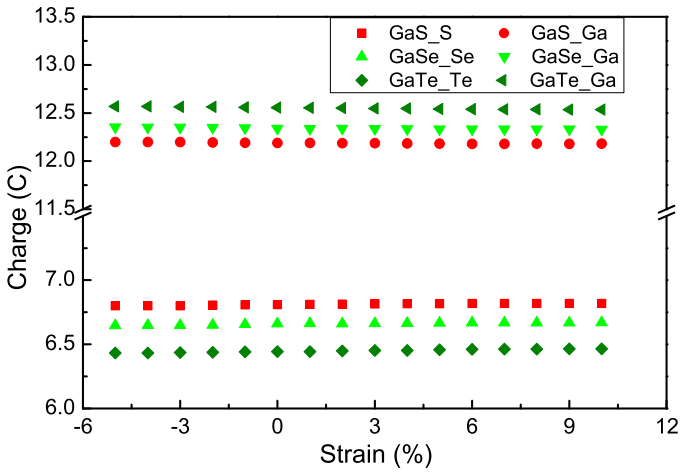

Fig. 6 (color online) Average Bader charge of Ga and X atoms for GaX monolayers as a function of strain. For respective GaX monolayer, the charges of Ga and X atoms are plotted in the same color.

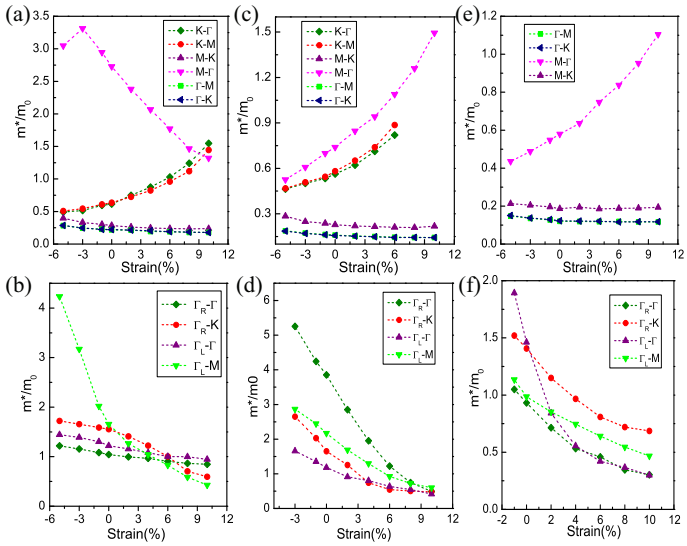

Fig. 7 (color online) The variation of effective masses (in units of electron mass m_0) of (a) electrons and (b) holes at high symmetry points of GaS with H-strain. (c),(d) and (e),(f) are the corresponding contents of GaSe and GaTe, respectively. Γ_R and Γ_L denote the Γ^* points at the right (to the K point direction) and left (to the M point direction) side of Γ point, respectively. The masses are labeled by the band extremum and the direction along which the mass is calculated.

Ga and X. This can be clearly seen from the binding energy listed in Table.2. Our PBE calculations show the binding energy is -6.963eV for GaS, -6.354eV for GaSe and -5.709eV for GaTe. Using the Bader charge analysis[38–40], we obtain the charge transfers from Ga to the chalcogen atoms. Each Ga atom loses 0.81 e in GaS sheet, 0.66 e in GaSe sheet and 0.44 e in GaTe monolayer. Due to the small charge transfers and elongated lattice constants, the binding energies of the GaS, GaSe and GaTe monolayers decreases. This, essentially, results in a weaker interaction between the M and X atoms and a decreasing band gap from GaS to GaTe, which agree well with our interpretation above.

Strain also has effect on the curvature of the band structure, reflected in a change of the effective masses of electrons and holes. Strain effects on effective masses of electrons and holes of GaX under H-strain are reported in Fig.7. The effective mass is calculated using $m = \hbar^2/(\partial^2 E/\partial k^2)$, and the k points closely approach the corresponding k-point, such as VBM and CBM. In Fig.7, Γ_R and Γ_L denote the Γ^* points at the right (to the K point direction) and left (to the M point direction) side of Γ point, respectively. The variation curve of effective mass of electron (or hole) at k-point to the k^*-point direction is labeled by $k-k^*$. For example, the curve labeled $\Gamma - M$ shows the evolution of the effective mass of electrons at Γ point to the M point direction. For simplification, only effect of H-strain on effective masses is taken into consideration in this work. The R point and S point, as a result, are equivalent to K point and M point, respectively.

Because the effective mass of electrons (holes) is determined by the dispersion of energy at the CBM (VBM), the jumping of CBM (VBM) will lead to a dramatic change of associated effective mass value. Take GaS as an example, when compressive strains is imposed, the CBM shifts from the Γ point to the M point and then to the K point. The mass of the electron at M point in the K direction is smaller the that at K point and is larger than that Γ. The jumping of CBM, essentially, results in a dramatic change of electron effective mass. For holes, the relevant VBM is near the Γ point without jumping to other points with strain. The masses of the holes at Γ_L point and Γ_R point show a similar variation trend and degrade slowly with increasing strain. This suggests that the hole effective mass of GaS will not change dramatically.

When under tensile strain more than 2%, it is worthy to note that the VBM and CBM locate at Γ^* and Γ point, respectively, and keep unchanged with increasing tensile strain. The electron effective mass for the band extremum at Γ is not very sensitive to strain while the hole effective mass decreases slowly with the tensile strain, implying maintenance of the quality of the conductivity. The modification of the band gap without significant alteration of the dispersion of the bands is very important for electronic applications. Furthermore, the electron mass is much smaller than that of holes regardless of applied stain, implying that the GaX will have important applications as an n-type material in field effect transistors. What's more, the electron effective mass of stretched GaX increases from GaS to GaTe, which suggests that GaS may show better trans-

port properties than GaSe and GaTe.

4 Conclusion

In summary, first-principles calculations are carried out to reveal the elastic and electronic properties of GaX (X = S, Se, Te) under strains. GaS, GaSe and GaTe show similar elastic, electronic and transport properties because they share the same atomic configuration and spatial symmetry group. The in-plane stiffness is found to decrease gradually with increasing atomic number of chalcogenide atoms, whereas the Poisson's ratio varies by a small amount among them. Upon application of strain, the band gaps of GaX can be modified and tuned in a relative large range. In the case of tensile strain, the band gaps of GaX decrease approximately linearly. While the variation of band gaps with compressive strain does not show linear feature because the conduction band maximum transfers among several high symmetry k-points. Besides, the A-strain and Z-strain exert similar effect on the band gap of GaX. Strain effects on effective masses of electrons and holes are reported in Fig.7. The jumping of CBM leads to dramatic changes of associated effective mass value. Besides, the plots of carrier effective mass also provide meaningful insight into the transport performance of strained monolayer GaX structures. In practice, these strains could potentially be realized by epitaxial growth on suitable substrates. Our results will be useful for interpretation the variable mobilities and transport properties of strained GaX electronic devices in experiments. Besides, the band gap of GaX can be modified by the tensile strain without significant change the dispersion of the bands, which is very important for electronic applications.

5 Acknowledgements

This work was supported by the National Natural Science Foundation of China under Grant No. 91233120 and the National Basic Research Program of China (2011CB921901).

References

1 K. Novoselov, D. Jiang, F. Schedin, T. Booth, V. Khotkevich, S. Morozov and A. Geim, *Proc. Natl. Acad. Sci. U.S.A*, 2005, **102**, 10451–10453.
2 A. K. Geim and K. S. Novoselov, *Nat. Mater.*, 2007, **6**, 183–191.
3 A. C. Neto, F. Guinea, N. Peres, K. S. Novoselov and A. K. Geim, *Rev. Mod. Phys.*, 2009, **81**, 109.
4 C. Jin, F. Lin, K. Suenaga and S. Iijima, *Phys. Review Lett.*, 2009, **102**, 195505.
5 H. L. Zhuang and R. G. Hennig, *J. Phys. Chem. C*, 2013, **117**, 20440–20445.
6 K. Novoselov, A. K. Geim, S. Morozov, D. Jiang, M. Katsnelson, I. Grigorieva, S. Dubonos and A. Firsov, *Nature*, 2005, **438**, 197–200.
7 Y. Zhang, Y.-W. Tan, H. L. Stormer and P. Kim, *Nature*, 2005, **438**, 201–204.
8 D. Elias, R. Nair, T. Mohiuddin, S. Morozov, P. Blake, M. Halsall, A. Ferrari, D. Boukhvalov, M. Katsnelson, A. Geim *et al.*, *Science*, 2009, **323**, 610–613.
9 H. Şahin and S. Ciraci, *Phys. Rev. B*, 2011, **84**, 035452.
10 Z.-H. Sheng, H.-L. Gao, W.-J. Bao, F.-B. Wang and X.-H. Xia, *J. Mater. Chem.*, 2012, **22**, 390–395.
11 Y. Wang, Y. Shao, D. W. Matson, J. Li and Y. Lin, *Acs Nano*, 2010, **4**, 1790–1798.
12 G. Cocco, E. Cadelano and L. Colombo, *Phys. Rev. B*, 2010, **81**, 241412.
13 G. Gui, J. Li and J. Zhong, *Phys. Rev. B*, 2008, **78**, 075435.
14 E. Scalise, M. Houssa, G. Pourtois, V. Afanasev and A. Stesmans, *Nano Res.*, 2012, **5**, 43–48.
15 W. S. Yun, S. Han, S. C. Hong, I. G. Kim and J. Lee, *Phys. Rev. B*, 2012, **85**, 033305.
16 H. Peelaers and C. G. Van de Walle, *Phy. Rev. B*, 2012, **86**, 241401.
17 Y. Ma, Y. Dai, M. Guo, C. Niu, Y. Zhu and B. Huang, *ACS Nano*, 2012, **6**, 1695–1701.
18 S. Tongay, J. Suh, C. Ataca, W. Fan, A. Luce, J. S. Kang, J. Liu, C. Ko, R. Raghunathanan, J. Zhou *et al.*, *Scientific Reports*, 2013, **3**, year.
19 P. Hu, L. Wang, M. Yoon, J. Zhang, W. Feng, X. Wang, Z. Wen, J. C. Idrobo, Y. Miyamoto, D. B. Geohegan *et al.*, *Nano Lett.*, 2013, **13**, 1649–1654.
20 D. J. Late, B. Liu, H. Matte, C. Rao and V. P. Dravid, *Adv. Func. Mater.*, 2012, **22**, 1894–1905.
21 D. J. Late, B. Liu, J. Luo, A. Yan, H. Matte, M. Grayson, C. Rao and V. P. Dravid, *Adv. Mater.*, 2012, **24**, 3549–3554.
22 S. Lei, L. Ge, Z. Liu, S. Najmaei, G. Shi, G. You, J. Lou, R. Vajtai and P. M. Ajayan, *Nano Lett.*, 2013, **13**, 2777–2781.
23 Y. Ma, Y. Dai, M. Guo, L. Yu and B. Huang, *Phys. Chem. Chem. Phys.*, 2013, **15**, 7098–7105.
24 H. L. Zhuang and R. G. Hennig, *Chem. Mater.*, 2013, **25**, 3232–3238.
25 P. E. Blöchl, *Phys. Rev. B*, 1994, **50**, 17953–17979.
26 J. P. Perdew, K. Burke and M. Ernzerhof, *Phys. Rev. Lett.*, 1996, **77**, 3865.
27 J. Heyd, G. E. Scuseria and M. Ernzerhof, *J. Chem. Phys.*, 2006, **124**, 9906.
28 H. J. Monkhorst and J. D. Pack, *Phys. Rev. B*, 1976, **13**, 5188–5192.
29 G. Kresse, *Phys. Rev. B*, 1996, **54**, 11–169.
30 A. Kuhn, A. Chevy and R. Chevalier, *Acta Crystallogr., Sect.B: Struct. Crystallogr. Cryst. Chem.*, 1976, **32**, 983.
31 A. Kuhn, A. Chevy and R. Chevalier, *phys. Status Solidi A*, 1975, **31**, 469–475.
32 M. Topsakal, S. Cahangirov and S. Ciraci, *Appl. Phys. Lett.*, 2010, **96**, 091912.
33 Q. Yue, S. Chang, J. Kang, S. Qin and J. Li, *J. Phys. Chem. C*, 2013, **117**, 14804–14811.
34 J. Kang, J. Li, F. Wu, S.-S. Li and J.-B. Xia, *J. Phys. Chem. C*, 2011, **115**, 20466–20470.
35 Y. Ding, Y. Wang, J. Ni, L. Shi, S. Shi and W. Tang, *Physica B*, 2011, **406**, 2254–2260.
36 J. Kang, S. Tongay, J. Zhou, J. Li and J. Wu, *Appl. Phys. Lett.*, 2013, **102**, year.
37 S. Bhattacharyya and A. K. Singh, *Phys. Rev. B*, 2012, **86**, year.
38 W. Tang, E. Sanville and G. Henkelman, *J. Phys.: Condens. Matter*, 2009, **21**, 084204.
39 E. Sanville, S. D. Kenny, R. Smith and G. Henkelman, *J. Comput. Chem.*, 2007, **28**, 899–908.
40 G. Henkelman, A. Arnaldsson and H. Jónsson, *Comput. Mater. Sci.*, 2006, **36**, 354–360.